In-situ fatigue damage analysis and prognostics of composite structures based on health monitoring data

20

Dimitrios Zarouchas, Nick Eleftheroglou
Structural Integrity & Composites Group, Delft University of Technology, Delft, The Netherlands

20.1 Introduction

There is a high demand of reliable predictions of the remaining useful life (RUL) of in-service composite structures. The predictions could be used as the leading indicator for an efficient maintenance planning, as well as they could prevent catastrophic failures due to unexpected phenomena, which may occur during service and dramatically degrade the mechanical properties of the structure. In order to achieve both, a deep understanding of the in-service damage accumulation process and a robust methodology to convert this information to RUL predictions are needed. Fatigue is the common term to describe the in-service damage accumulation process and it occurs when loads are applied to the structure over time.

Fatigue of composite structures has been in the center of the research activities the last four decades, where the research community has tried to model the phenomenon of damage accumulation and develop predictive tools. Extensive experimental campaigns for different material types and lay-up configurations and a considerable number of models emerged from those activities and revealed that the fatigue damage process is a multistate degradation procedure where several damage mechanisms occur, interact, act synergistically, and lead the structure to final failure.

The idea of the multistate process goes back to the 1980s, where Reifsneider et al. described the damage accumulation as a three-stage process [1]. According to Ref. [1] the prediction of strength and life of a composite structure should be based on the actual damage mechanisms. Ever since, the researchers have focused on developing prediction models implementing phenomenological and progressive damage approaches [2–10]. However, only the progressive damage approaches consider to some extent the damage mechanisms. Despite the efforts and the progress made in the field, it was clear, rather early, that a universal model, which can cover all types of composite materials, lay-up configurations and loading scenarios is very difficult to be established.

Fatigue Life Prediction of Composites and Composite Structures. https://doi.org/10.1016/B978-0-08-102575-8.00020-6

The last decade, several researchers revisited the original idea proposed by Reifsneider and focused on understanding and unfolding the fatigue damage process. A common understanding has been established regarding the three states of damage development during fatigue of unidirectional, cross-ply, and angle-ply composites [11–14];

- state I—damage initiation by formation of matrix cracking with numerous micro-cracks developed within the ply-level until saturation,
- state II—delamination onset, growth and mitigation to adjacent plies,
- state III—damage progression in the matrix-fiber interface resulting in fiber debonding, fiber breakage, and pull-out, which eventually leads to the final failure.

The precise damage accumulation sequence depends on the material properties of the composite's constituents, the exact layup, the defects induced during manufacturing, the loading profile, and the environmental conditions in which the structure operates. Additionally, the inhomogeneous nature of the composite material and the stochastic activation of different damage mechanisms should also be taken into account making the damage process a very complex phenomenon to study. When it comes to analyze their effect on the damage process and consequently on the RUL, all these parameters should be considered as uncertainties.

Uncertainty quantification and analysis of its impact on the RUL, via modeling the stochastic process of damage accumulation, is nowadays possible by using available probabilistic mathematical algorithms and the increase of computational power. A potential solution to predict the RUL of composite structures, taking into account uncertainties, comes from the field of prognostics where machine learning algorithms, health monitoring data, and mechanics blend together to create a structural prognostics framework. The prognostic framework originates from the condition monitoring of rotating machinery. The need to estimate the wear degradation rates and to reduce the down time (or increase the availability) was the main driven force behind the development of this framework [15]. The main advantage over the current methodologies is that it can provide predictions in real time.

A large amount of health monitoring data, using different sensing technologies, can be acquired and further analyzed in order to assess the degradation level and predict the RUL of composite structures in-service. So, a more suitable approach for prediction of the RUL is to adapt and update in real-time a probabilistic model that can relate the health monitoring data with the degradation process. In this direction, it is possible to make more accurate predictions since these models take into account the uncertainties. The core of a prognostic framework is the involved algorithms and can be categorized as follows [16, 17]:

- Physics-based algorithms
- Data-driven algorithms
- Hybrid algorithms

The physics-based prognostic algorithms assume that a physical model, able to describe the degradation process, is available. To this direction, Chiachio et al. and Corbetta et al. utilized a Bayesian filtering framework that incorporates information

from empirical damage models and health monitoring data in order to predict the RUL of composite [18–20]. They used state-of-the-art empirical models for matrix cracking, delaminations and crack growth to predict through the use of particle filtering the future damage states and thus estimate the RUL. However, the parameters of those empirical models, that is, the fitting parameters of Paris power law relation, depend on the type of failure, loading case, geometry, and stacking sequence, limiting the applicability of these models to coupons rather than to complex composite structures [21, 22].

In contrast, the main idea behind prognostic data-driven algorithms is to use health monitoring training data from the studied component (independent on its complexity in terms of loading conditions, geometry, etc.), in order to estimate the parameters of a model, which provides the mathematical framework to describe the phenomenon of interest, that is, the fatigue damage accumulation process in composite structures. Then, based on the trained model a probability density function of the RUL can be determined. A crucial factor on the successful development of a structural prognostic framework is the utilization of a stochastic model that fits on the degradation process of the structure. An appropriate model should demonstrate the capability to relate the fatigue damage process with its mathematical concept.

Characteristic examples of data-driven prognostic approaches for composite materials/structures are presented hereafter. Liu et al. [23] utilized Gaussian processes, as a mathematical model, to perform nonlinear regression. Gaussian process was trained with acoustic emission (AE) data and Lamb wave signals in order to estimate the RUL of composite beams. By comparing the RUL estimations of Lamb wave signals and a data, it can be seen that Lamb's RUL estimations were better than AE's RUL estimations. The same research team proposed a prognostic methodology, which consisted of real-time sensor signals from strain gages, direct cross-correlation analysis, and a Gaussian process trained with off-line data to perform the nonlinear regression prognostic task [24]. Notched carbon/epoxy composite specimens under fatigue loading were used. Eleftheroglou and Loutas [25] and Eleftheroglou et al. [26] proposed the use of a multistate degradation model, the nonhomogenous hidden semi-Markov model (NHHSMM), for the in-situ prognostics of open hole carbon/epoxy specimens under fatigue loading. They used AE and strain measurements to estimate the parameters of the NHHSMM and successfully used it to obtain RUL estimates in unseen data with uncertainty quantification. In Loutas et al. [27] two data-driven prognostic models, NHHSMM and Bayesian neural networks (BNNs), utilizing AE measurements, were compared via several prognostic performance metrics. Fatigue tests were performed in open-hole carbon/epoxy specimens. The NHHSMM clearly exceled the performance metrics at this study. The aforementioned case studies represent some prognostic models that are encountered in the literature on application to composite structures. Finally, to the best knowledge of the authors there is no hybrid approach available in the literature for the structural prognostics of composites.

Based on the available stochastic models, one of the most promising stochastic model is the NHHSMM because it supports multistate degradation modeling and it can be related to the fatigue damage accumulation process. The model is presented in Section 20.3.

20.2 Structural health monitoring

Structural health monitoring (SHM) can be described as the process of implementing a damage detection strategy for load-bearing structures [28, 29]. This process involves the observation of the mechanical response and the integrity assessment of the structure by using permanently installed sensors. The sensors record data periodically or continuously over the in-service life of the structure, damage-sensitive features are extracted from these data and statistical analysis is performed to determine the health state of the structure (diagnostics). Extensive research has been performed the last two decades in the field of SHM resulting in a large amount of sensing technologies, which can be used for SHM, exist nowadays.

AE, guided ultrasonic waves, electromechanical impedance, fiber Bragg grating techniques are among the most popular sensing technologies which can serve the purpose of the SHM [30–35]. These techniques have been employed in most cases solely, while, when a second technique was used, it was mainly for cross-correlation of the observations. In that case, the techniques for the cross-correlation process were mainly nondestructive testing (NDT) techniques, such as C-Scan and CT-tomography. A common practice is to scan the specimen before the test, during the test by interrupting the loading, and after the final specimen failure. CT-tomography is proved to be the most powerful equipment that maps in 2D and 3D the failure zones and can provide quantitative information about the damage modes involved (see chapter Lars Mikkelsen). However, in case that scan needs to take place periodically during the life time of the specimen, the specimen should be removed from the test bench at every given number of fatigue cycles, compromising the validity of the test. Besides the technical challenges related to the precise repetition of the specimen's installment in the test bench, it is expected that the fatigue damage process will also be interrupted (see Chapter Vassilopoulos—interrupted fatigue).

Thus, it is crucial for the validity of the experimental data to select techniques that serve the goals of the study. For example, if the main goal of an experimental campaign is to study the damage accumulation process from the beginning until the end of life of the structure without stopping the loading sequence, then techniques, which can continuously measure and collect data such as AE and/or fiber Bragg grating, should be selected. However, it is worth to mention that each technique has different sensitivity to different failure mechanisms and a technique, which is able to monitor each single damage mechanism, does not exist. Farrar and Worden addressed this statement and concluded that a successful implementation of SHM process requires a synergistic and multidisciplinary approach [29]. Toward that several studies have been performed and the researchers explored the benefit of sensing and data fusion for diagnostic purposes [36, 37].

During the case study that is presented in the following sections two sensing technologies were used; AE and digital image correlation (DIC). The main reason for selection of these techniques, besides the fact that they can collect data without interrupting the fatigue tests, is that the measurements are related to different structural scales. The AE data relates to damage mechanisms occurred in the microscale, since the AE sensors are capturing and recording in the data acquisition system elastic

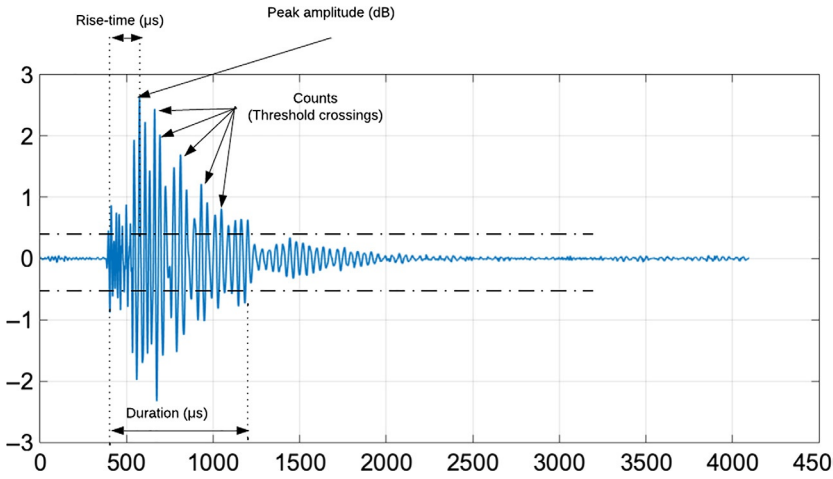

Fig. 20.1 A representative AE signal.

transient waves propagating into the structure after the release of energy, due to formation of new or propagation of existing damage. Commercial systems exist and they can perform parametric analysis by quantifying AE features such as amplitude, duration of the wave, rise time, and energy or record the entire waveform. A typical AE waveform and its features are presented in Fig. 20.1.

The DIC technique was employed in order to measure full field surface displacements at the macroscale. However, it should be noted that it is very difficult to use DIC as sensing technique in a SHM approach, especially for not stationary infrastructure, due to high sensitivity in vibration, which would compromise the quality of the images taken by the cameras. The main reason of utilizing this technique was to collect strain data and use it as health monitoring data for the data fusion approach as it is presented in the following sections.

20.3 Non homogeneous hidden semi-Markov model

The fatigue damage accumulation process of a composite structure is a multistate process where the exact interaction and synergy of different damage mechanisms are not known, and thus we can assume that this process is hidden. Moreover, as health monitoring data is the result of this process, it is acceptable to conclude that the data can be used to unfold the fatigue damage accumulation process. Driven by this rational, the hidden Markov model, as data-driven algorithm, is an excellent candidate, offering the mathematical background to build a prognostic framework. However, this early version of the Markov model assumes an exponential distribution of each state's duration, which is not always the case, especially for composite structures where the duration of damage state, that is, the formation of matrix cracks, may be different from the duration of the next damage state, that is, the formation and the development

of delaminations. On the other hand, the hidden semi-Markov model removes this restriction and allows the unconstrained modeling of each state duration. Nevertheless, both models have limitations about the transition process from one state to another. They are considered to be independent of the aging process of the system, which is not the case for composite structures.

Moghaddass et al. extended the hidden semi-Markov model to the NHHSMM where the state transition process depend on the current state, the time spent on this state and the total aging process of the structure [38, 39]. This model fits very good to the fatigue damage accumulation process because as the damage always increases over time it can be implied that the probability of state transition to higher damage states increases as well.

The definition of a series of elements is required in order to describe the NHHSMM;

- The number of possible discrete degradation health states (N),
- the transition diagram which defines the connectivity between the states and the allowed transitions,
- the transition rate's statistical function (λ),
- the observations, that is, the health monitoring data feature(s) $y_{1:t}(\mathrm{y}_{1:\mathrm{t}})$, and
- the number of discrete feature values (m) after the observations quantization.

The number of hidden states refers to the number of discrete levels of degradation. In a maximum likelihood estimation (MLE) approach, Moghaddass et al. [38] demonstrated a procedure to maximize $\Pr(y^{(k)}|\boldsymbol{\theta})$, that is, define the model parameters $\boldsymbol{\theta}$ which maximize the probability of the K available for training observation sequences $\boldsymbol{y}^{(\boldsymbol{k})}$.

$$\begin{aligned} L\left(\theta, \boldsymbol{y}^{(\mathbf{1}:\boldsymbol{K})}\right) &= \prod_{k=1}^{K} Pr\left(\boldsymbol{y}^{(\boldsymbol{k})} | \boldsymbol{\theta}\right) \xrightarrow{L'=log(L)} L'\left(\boldsymbol{\theta}, \boldsymbol{y}^{(\mathbf{1}:\boldsymbol{K})}\right) \\ &= \sum_{k=1}^{K} \log\left(Pr\left(\boldsymbol{y}^{(\boldsymbol{k})} | \boldsymbol{\theta}\right)\right) \Rightarrow \\ \boldsymbol{\theta}^{*} &= arg \max_{\boldsymbol{\theta}} \left(\sum_{k=1}^{K} \log\left(Pr\left(\boldsymbol{y}^{(\boldsymbol{k})} | \boldsymbol{\theta}\right)\right)\right) \end{aligned} \tag{20.1}$$

Utilizing Baum's auxiliary function, the above optimization task is reduced to a set of independent equations for the reestimation of the elements of $\boldsymbol{\Gamma}$, $\boldsymbol{B}$. The mathematical treatment leads to two reestimation equations:

$$\begin{aligned} \omega_{1,1}^{r}\left(\boldsymbol{\theta}_{\boldsymbol{old}}, \boldsymbol{\theta}\right) &= \sum_{k=1}^{K} \Pr\left(\boldsymbol{y}^{(\boldsymbol{k})} | \boldsymbol{\theta}_{\boldsymbol{old}}\right)^{-1} \\ &\times \sum_{j=1}^{N} \sum_{a=0}^{d_k} \sum_{d=1}^{d_k - a} \log\left(\varepsilon_{a}^{(k)}(r, j, d | \boldsymbol{\theta}) \times \kappa_{a}^{(k)}\left(r, j, d, \boldsymbol{y}^{(\boldsymbol{k})} | \boldsymbol{\theta}_{\boldsymbol{old}}\right)\right) \end{aligned} \tag{20.2}$$

where $1 \le r \le N-1$ giving thus $N-1$ equations and

$$b_i(w) = \frac{\sum_{k=1}^{K}\left(\Pr\left(\boldsymbol{y}^{(k)}|\,\boldsymbol{\theta_{old}}\right)^{-1} \times \sum_{t=1}^{d_k}\gamma_t\left(i,\boldsymbol{y}^{(k)}|\,\boldsymbol{\theta_{old}}\right)\delta_{O_t^{(k)},w}\right)}{\sum_{k=1}^{K}\left(\Pr(\boldsymbol{y}^{(k)}|\,\boldsymbol{\theta_{old}})^{-1} \times \sum_{t=1}^{d_k}\gamma_t(i,\boldsymbol{y}^{(k)}|\,\boldsymbol{\theta_{old}})\right)} \tag{20.3}$$

where $1 < w < m$ and the terms $\varepsilon_a^{(k)}(i,j,d|\,\boldsymbol{\theta})$, $\kappa_a^{(k)}(r,j,d,\boldsymbol{y}^{(k)}|\,\boldsymbol{\theta_{old}})$, and $\gamma_t(i,\boldsymbol{y}^{(k)}|\,\boldsymbol{\theta_{old}})$ are introduced in order to simplify the MLE process and are defined as follows:

$$\varepsilon_a^{(k)}(\mathrm{i,j,d}|\,\boldsymbol{\theta}) = \Pr\left(X_n = j, t_{a+d-1}^{(k)} < T_n \le t_{a+d}^{(k)} | \, X_{n-1} = i, t_{a-1}^{(k)} < T_{n-1} \le t_a^{(k)}, \boldsymbol{\theta}\right),$$

$$\kappa_a^{(k)}\left(\mathrm{r,j,d},\boldsymbol{y}^{(k)}|\,\boldsymbol{\theta_{old}}\right) = \Pr\left(X_n = j, t_{a+d-1}^{(k)} < T_n \le t_{a+d}^{(k)}, X_{n-1} = i, t_{a-1}^{(k)} < T_{n-1} \le t_a^{(k)}, \boldsymbol{y}^{(k)}|\,\boldsymbol{\theta_{old}}\right),$$

$$\gamma_t\left(i,\boldsymbol{y}^{(k)}|\,\boldsymbol{\theta_{old}}\right) = Pr\left(Q_t = i, \boldsymbol{y}^{(k)}|\,\boldsymbol{\theta_{old}}\right),$$

with X_n being the state of the component after the nth transition, T_n the time of the nth transition, Q_t the current hidden state, and $t_i^{(k)}$ the ith observation time point of the k_{th} observation/SHM data sequence $\boldsymbol{y}^{(k)}$.

The MLE approach begins with a random initialization of $\boldsymbol{\Gamma}$, $\boldsymbol{B}$, and via the use of the reestimation Eqs. (20.2) and (20.3) and it aims to the iterative maximization of the $\sum_{k=1}^{K}\log\left(\Pr\left(\boldsymbol{y}^{(k)}|\,\boldsymbol{\theta}\right)\right)$ value. This procedure concludes to a parameter vector $\boldsymbol{\theta}$ which describes the most probable model for a given training data set.

Regarding the prognostics, the mean RUL is the quantity of interest in a condition-based monitoring framework. It can be estimated via Eq. (20.4) as the integral of the conditional reliability function $R(t\,|\,y_{1:t_p}, L > t_p, M) = Pr(L > t\,|\,y_{1:t_p}, L > t_p, M)$, that is, the probability that the composite material/component continues its operation after a time point t (less than life-time L) further than the present time t_p. This is a definition, which is conditional on SHM data, that is, the observation sequence $y_{1:t_p}$. Details on the calculation of the conditional reliability function can be found in Ref. [25].

$$\widehat{RUL}\left(t|\,y_{1:t_p}, L > t_p, M\right) = \int_0^{\infty} R\left(t+\tau|\,y_{1:t_p}, L > t_p, M\right)d\tau \tag{20.4}$$

In prognostics, an estimate of the uncertainty that follows the mean RUL estimation is of utmost importance, in order to give a confidence of the predicted mean value. The calculation of confidence intervals is based on the calculation of the $a\%$ and $(1-a)\%$ lower and upper percentiles, respectively. It can be easily proved that the cumulative distribution function (CDF) for RUL can be defined at any time point utilizing the conditional reliability according to the following:

$$Pr\left(RUL_{t_p} \le t|\,y_{1:t_p}, M\right) = 1 - R\left(t+t_p\,\middle|\,y_{1:t_p}, M\right) \tag{20.5}$$

20.4 Prognostics framework

The main goal of a prognostics framework is to estimate the composite structure's RUL by providing a probability density function. The framework consists of the training and online process, as presented in Fig. 20.2.

The objective of the training process is to collect health monitoring data, extract features that characterize the degradation process, and estimate the model's parameters. Based on the available training data features the parameters θ of the mathematical model that is utilized to provide the RUL predictions are estimated. After training the respective NHHSMMs, health monitoring data observations from an unseen case (online process) may feed the model, after similar future extraction, and obtain the mean RUL estimations (prognostics output) and the associated 90% confidence intervals.

20.4.1 Data processing and feature extraction

In the framework of this study, AE and strain data are used. The available SHM data can be divided to training and testing sets. However, the raw AE and DIC data include noise so a feature extraction process is required in order to produce features with strong prognostic suitability. A set of three metrics, monotonicity, prognosability, and trendability, has been proposed in the relevant literature, which can be used as feature design properties [40–43]. Monotonicity characterizes a parameter's general

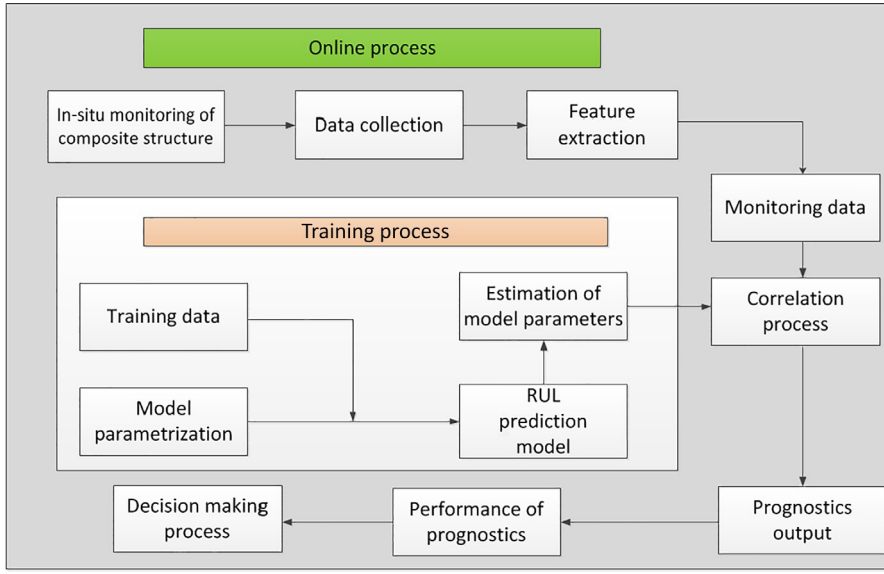

Fig. 20.2 The prognostics framework for prediction of the remaining useful life.

increasing or decreasing trend, prognosability measures the spread of a parameter's failure value and finally, trendability indicates whether degradation histories of a specific parameter have the same underlying trend.

In this study, the feature extraction process is based on monotonicity since a feature that is sensitive to the degradation process is desirable to have a monotonic trend [41, 42, 44]. Prognosability is excluded from the present feature extraction process since NHHSMM dictates that the last observation of the monitoring data must be unique and common for all the degradation histories. Finally, the feature extraction process does not take into account the influence of trendability. The main reason is that we wanted to benchmark the data fusion process against AE and DIC data keeping the computational complexity as low as possible.

A second key element of the NHHSMM is that the monitoring data's domain should be discrete. Different methods, such as vector quantization and clustering can be used to discretize the available monitoring data [45]. In this chapter, the unsupervised k-means algorithm is used to cluster and discretize the features extracted from the SHM data. The target of using k-means algorithm is to find the optimal number of discrete levels, which delivers features with maximum monotonicity. To quantify the monotonicity the modified Mann-Kendall (MMK) criterion is introduced in the following equation.

$$\mathrm{MMK} = \frac{\sum_{i=1}^{D}\sum_{j=1,j>i}^{D}\left(t_j - t_i\right)\cdot \mathrm{sgn}\left(y\left(t_j\right) - y\left(t_i\right)\right)}{\sum_{i=1}^{D}\sum_{j=1,j>i}^{D}\left(t_j - t_i\right)}\cdot 100\% \tag{20.6}$$

where $y(t_i)$ the feature value at time of measurement t_i, D the number of measurements and $sgn(x) = \left\{\begin{array}{c} -1 \text{ if } x<0 \\ 0 \text{ if } x=0 \\ 1 \text{ if } x>0 \end{array}\right\}$.

The advantages of the MMK criterion, over the classical Mann-Kendal criterion [30], are explained in the following:

- Mann-Kendal (MK) values have not any informative meaning. For example, in the current case study the MK values' range is $(10^5, 4\times10^5)$. However, MMK value as defined in Eq. (20.6) expresses a percentage of monotonicity in the range $[-1.1]$. If MMK $=1$ the degradation history is strictly increasing, if MMK $=-1$ the degradation history is strictly decreasing. In any other case the degradation history is not strictly monotonic.
- Based on the MMK criterion each degradation history has the same monotonicity weight. On the other hand, the classical MK criterion is biased since a longer degradation history gives a higher MK value.

The objective of the feature extraction process as implemented in this study, is to obtain descritized degradation histories with the as high monotonicity as possible using features from AE data, DIC data, and fused ones.

20.4.2 Data fusion process

The health monitoring data can be collected by using different sensing technologies. The process of extracting information from different monitoring techniques and integrate them into a consistent, accurate and reliable data set is known as data fusion and it has been already successfully applied to damage diagnostics [46–48]. In principle, data fusion can be implemented in three levels:

- raw multi-sensor data fusion,
- feature-level fusion,
- decision-level fusion.

Raw data fusion should be treated with caution as sensor recordings may have different acquisition, prefiltering and amplification settings. Additionally, raw data fusion needs to have as input commensurate data. As a result, the feature-level and decision-level fusion are the more commonly used.

Combining features extracted from different sensors or monitoring techniques and integrating them into a single feature is known to enhance the diagnostics performance [49]. Data fusion for structural prognostics purposes has never been attempted according to the author's best knowledge. It is expected that the prognostic performance should be improved when fusing SHM data from various monitoring techniques.

The fusion scheme receives as inputs the quantized AE and DIC features, where the following equation explains the rationale behind fusing process.

$$f_t(DIC, AE) = \sum_{j=0}^{M} \sum_{i=0}^{i+j \le M} a_{ij} \cdot DIC^j \cdot AE^i \tag{20.7}$$

where f_t is the fused output feature, a_{ij} are constant coefficients that control the weight of the exponential DIC and AE features' product and M the maximum polynomial degree power that these features can use. The MMK criterion, Eq. (20.7), is adopted to enable the data fusion process and is expressed in Eq. (20.8). MMK is used as an objective function to be maximized and thus determine which polynomial degree M and constant coefficients a_{ij} give the most monotonic fused feature.

$$\mathrm{MMK}\left(a_{ij}, M\right) = \frac{\left[\sum_{k=1}^{K} \sum_{i=1}^{d_k} \sum_{j=1, j>i}^{d_k} \left(t_j^{(k)} - t_i^{(k)}\right) \cdot \mathrm{sgn}\left(f_j^{(k)}(a, M) - f_i^{(k)}(a, M)\right)\right]}{\left[\sum_{k=1}^{K} \sum_{i=1}^{d_k} \sum_{j=1, j>i}^{d_k} \left(t_j^{(k)} - t_i^{(k)}\right)\right]} \cdot 100\% \tag{20.8}$$

where K is the number of available training degradation histories (e.g., the number of tested specimens), $f_i^{(k)}$ the fused feature value at time of measurement $t_i^{(k)}$ for the kth specimen, d_k the number of the kth specimen's measurements and

$$sgn(x) = \left\{ \begin{array}{c} -1 \, if \, x < 0 \\ 0 \, if \, x = 0 \\ 1 \, if \, x > 0 \end{array} \right\}.$$

The constant polynomial coefficients a_{ij}, for each polynomial degree M, are based on the optimization problem described in Eq. (20.9) with the monotonicity obtained by the MMK criterion as the objective function. For the aforementioned optimization problem, different optimization techniques were used, that is, Nelder-Mead, neural networks, particle swarm optimization (PSO), genetic algorithms, and OptQuest nonlinear programs (OQNLP). For this exercise, it was found that OQNLP is the most efficient optimization technique regarding the computational time of the parameters α^*_{ij} and M. The unconstrained optimization problem is formulated as

$$\alpha_{ij}^* = \arg\max_{a_{ij}} \left(\mathrm{MMK}\left(a_{ij}, \mathrm{M}\right) \right) \tag{20.9}$$

In conclusion, the outputs of the proposed data fusion methodology are the optimum polynomial degree M and the optimum constant coefficients a_{ij} based on the MMK monotonicity, Eq. (20.9).

20.5 Case study

A laminate with $[0/\pm45/90]_{2s}$, lay-up were manufactured from a Hexcel AS4/8552 carbon-epoxy UD prepreg using hand lay-up, with a debulking procedure performed after every three plies. Afterwards, the laminate was cured using the autoclave process with a curing cycle as recommended by the manufacturer of the prepreg. The laminate was cut in rectangular specimens of 300×30 mm using a Proth Industrial liquid-cooled saw and a central hole of 6 mm was drilled. Seven open-hole were used in the experimental campaign. These specimens were subjected to fatigue loading with maximum amplitude 90% of the static tensile strength ($F_{ult} = 42.66$ kN), $R = 0$ and $f = 10$ Hz. The tests were executed in a MTS 100 kN universal testing machine and they run up to failure. An AE system was used in order to perform AE measurements. Fig. 20.3 presents the schematic representation of the experimental set-up and the data acquisition process. Table 20.1 presents the cycles to failure for the tested specimens.

20.5.1 Strain data feature extraction

The DIC technique enabled strain measurements in the entire surface of the specimen.

Two Grasshopper3 5.0 MP Mono with Apo-Xenoplan 1.4/23 mm lenses and strain resolution of 200με were used while the analysis of the data was performed using the

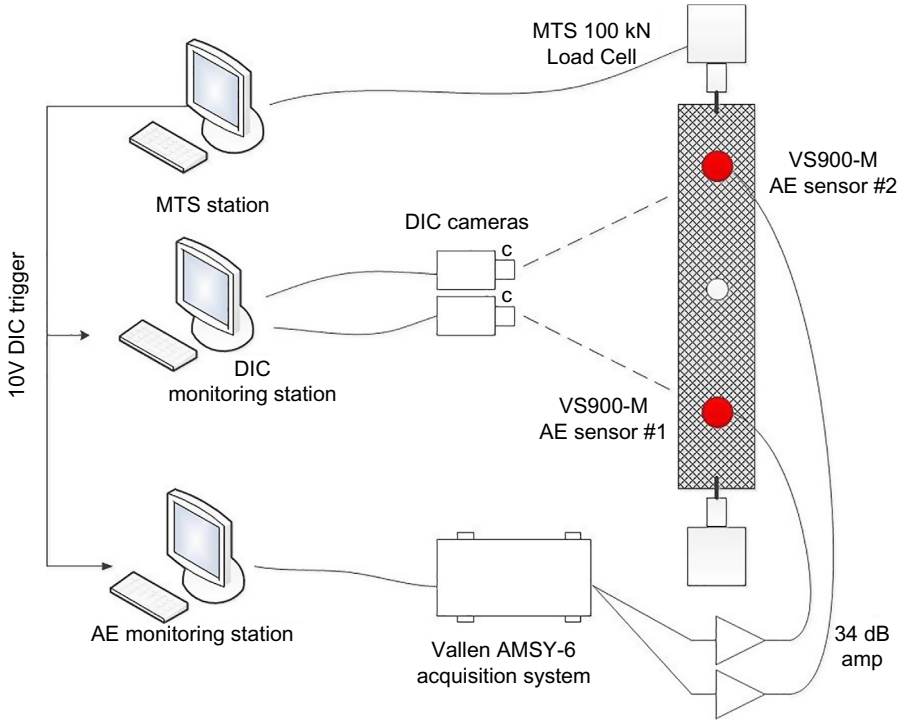

Fig. 20.3 The schematic representation of the experimental set-up.

Table 20.1 Cycles to failure of the open-hole specimens

Coupon	Fatigue test conditions	Cycles to failure
Specimen 01	$R=0$	63122
Specimen 02	$F=10$ Hz	24239
Specimen 03	$\sigma_{max}=90\%$ UTS	22400
Specimen 04	$[0/\pm45/90]_{2s}$	24015
Specimen 05		13658
Specimen 06		25101
Specimen 07		29258

VIC-3D software supplied by the Correlated Solutions. Fig. 20.4 presents the axial strain distribution, strain in the load direction, as calculated at the maximum loading during the fatigue test of specimen02.

Based on the analytical model of Lekhnitskii [50], which calculates the effect of a notch on the stress/strain distribution, the green rhomboid point (half a diameter distance for the hole center in the transverse direction), highlighted at the picture of 0 cycles, was chosen as the critical point to extract the axial strains. Fig. 20.5 presents the seven axial strain degradation histories, which were extracted for the aforementioned critical point.

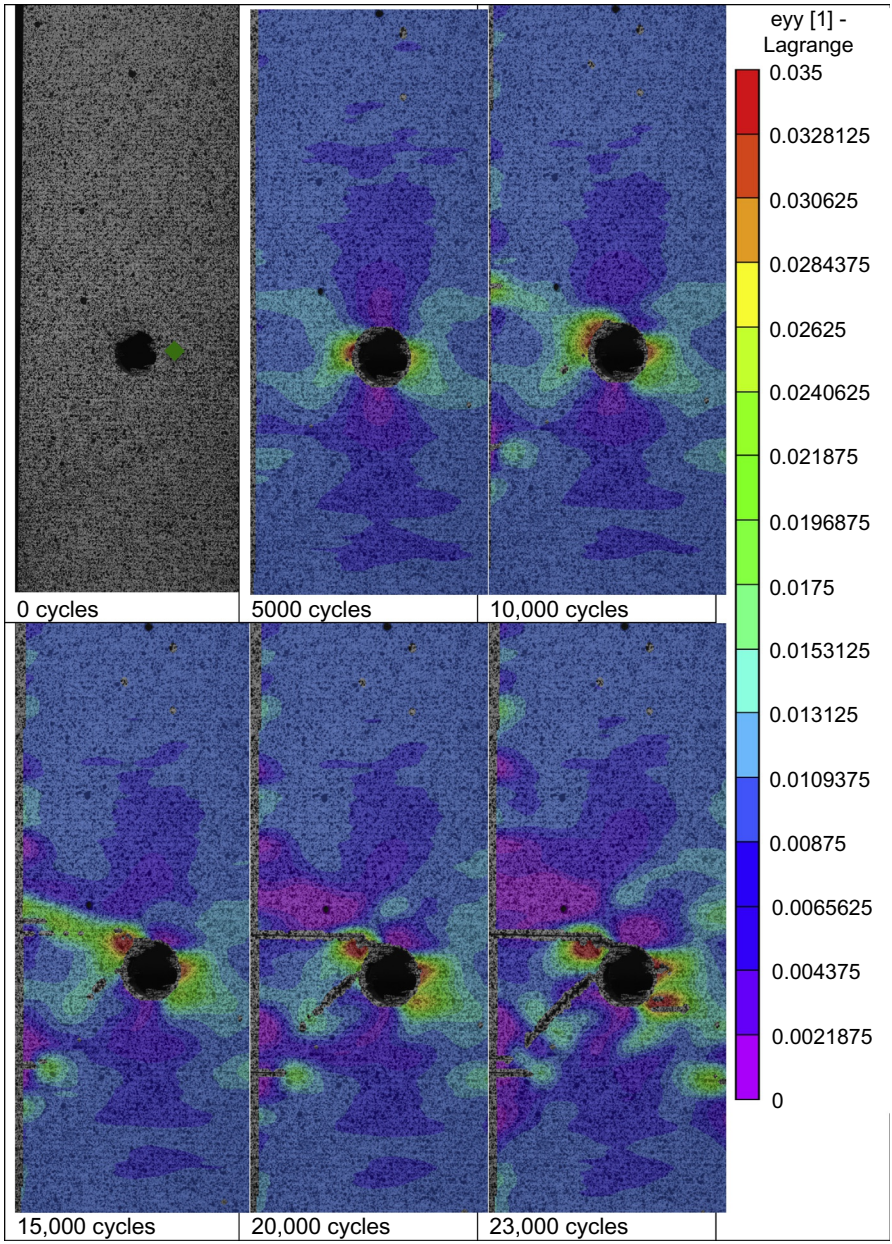

Fig. 20.4 Axial strain distribution of specimen02.

As discussed earlier, the final data feature should be presented in a discrete form by the clusters V that can be calculated using the MMK criterion. The MMK converges for the number of clusters V equal to 25 for the data, as presented in Fig. 20.6. Fig. 20.7 presents the final clustered axial strain data after the thresholding process.

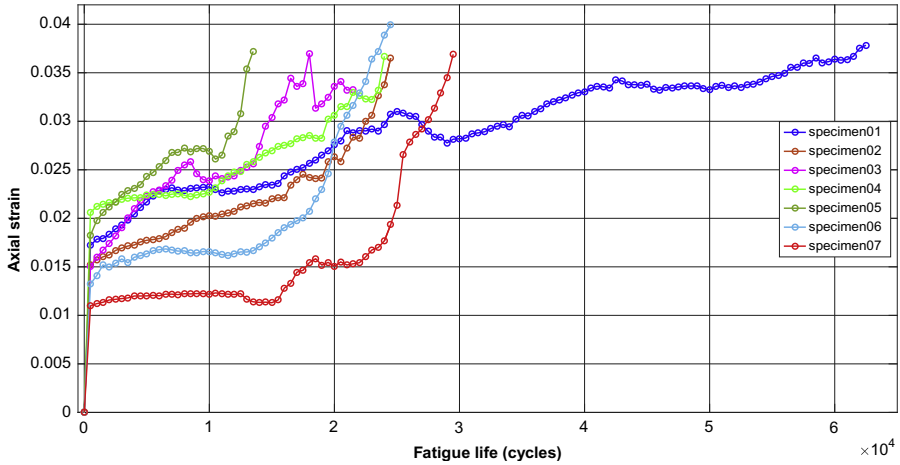

Fig. 20.5 Axial strain degradation histories of seven open-hole specimens.

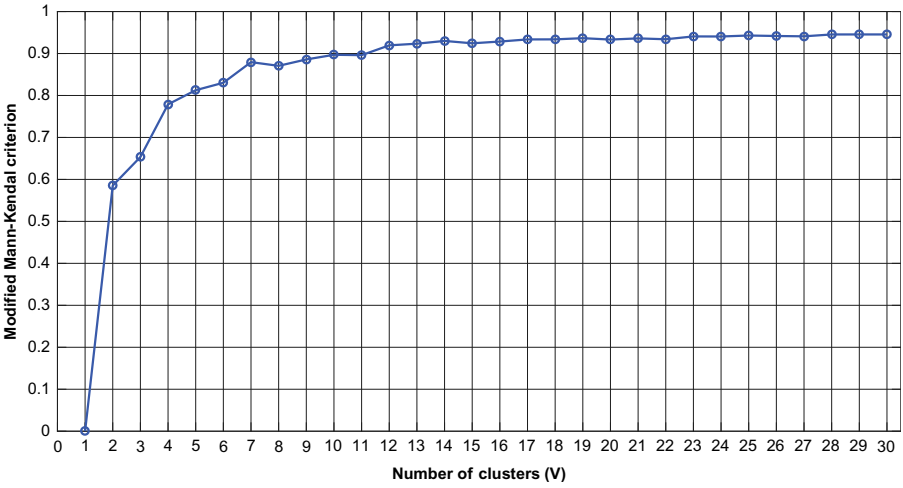

Fig. 20.6 MMK monotonicity convergence of DIC data vs the number of clusters (V).

20.5.2 AE feature extraction

An AMSY-6 Vallen, 8-channel AE system with four parametric input channels was used in this study. Two wide-band piezoelectric sensors, VS-900 M, with an external 34 dB preamplifier and a band-pass filter of 20–1200 kHz, were clamped on the specimens using a mechanical holder. In order to increase the conductivity between the AE sensors and the specimen, grease was applied on the surface of the sensors and pencil break tests were conducted before each experiment so as to ensure the conductivity. One parametric input channel was used to record the load and correlate it to the AE

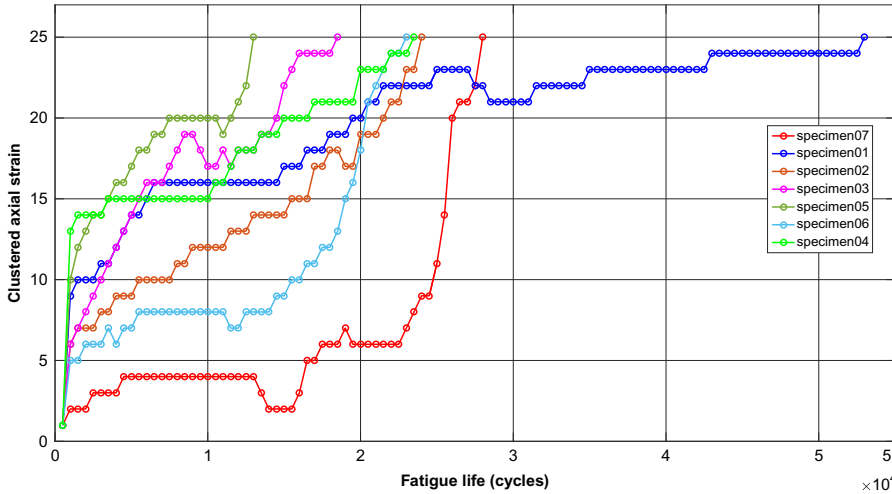

Fig. 20.7 Clustered axial strain degradation histories of seven open-hole specimens.

data. The AE acquisition threshold was set to 50 dB and the AE data set for each AE hit contained the duration (μs), rise time (μs), peak amplitude (dB), energy (1 eu = 10^{-18} J), the number of threshold crossings, and ratio rise time to amplitude.

1/A (1/amplitude) was found to have the highest monotonic observation sequences and it was selected as the AE feature to use. Similar to strain measurements, 1/A was calculated cumulatively in periodic time windows of 500 cycles. The respective degradation histories for seven specimens are shown in Fig. 20.8.

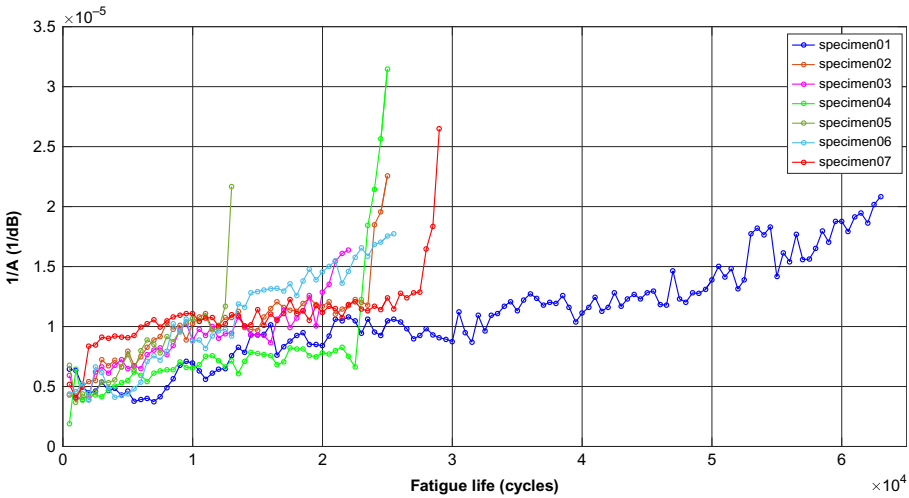

Fig. 20.8 AE degradation histories of seven open-hole specimens.

Although the MMK monotonicity converges for number of clusters ≥ 18, see Fig. 20.9, $V = 25$ was selected for the AE data equal to the number of clusters for strain data. This way, the data fusion process becomes more efficient as the normalization of the AE and DIC features is avoided. Fig. 20.10 presents the final clustered AE data.

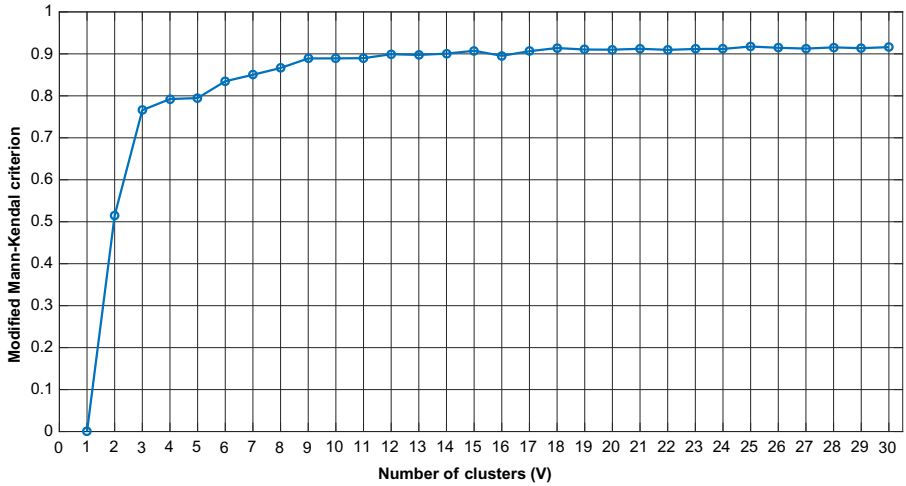

Fig. 20.9 MMK monotonicity convergence of AE data vs the number of clusters (V).

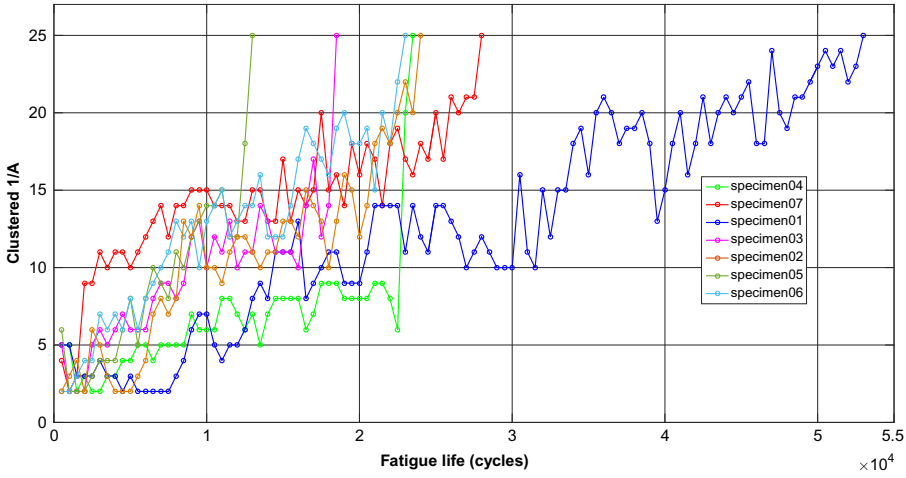

Fig. 20.10 Clustered AE degradation histories of seven open-hole specimens.

20.5.3 Data fusion of AE and strain data

The results of the optimization study, Eq. (20.9), are presented for various polynomial degrees M in Fig. 20.11. The MMK monotonicity converges for a polynomial degree $M \geq 5$. Therefore, the polynomial degree is selected as $M = 5$.

For the selected polynomial degree $M = 5$, Table 20.2 summarizes the optimization results regarding the constant coefficients a_{ij}.

The fused features for polynomial degree $M = 5$ and the aforementioned polynomial coefficients a_{ij} are shown in Fig. 20.12.

Fig. 20.13 presents the MMK monotonicity for each SHM feature, that is, AE, DIC, and fused data and it is observed that the fused data have the highest monotonic rate. The data fusion process is presented in Fig. 20.14.

20.5.4 RUL estimations

Seven degradation histories $\mathbf{Y} = [\mathbf{y}^{(1)}, \mathbf{y}^{(2)}, \ldots, \mathbf{y}^{(7)}]$ were available for each SHM technique (AE, DIC, and fused data). The training dataset employs six degradation

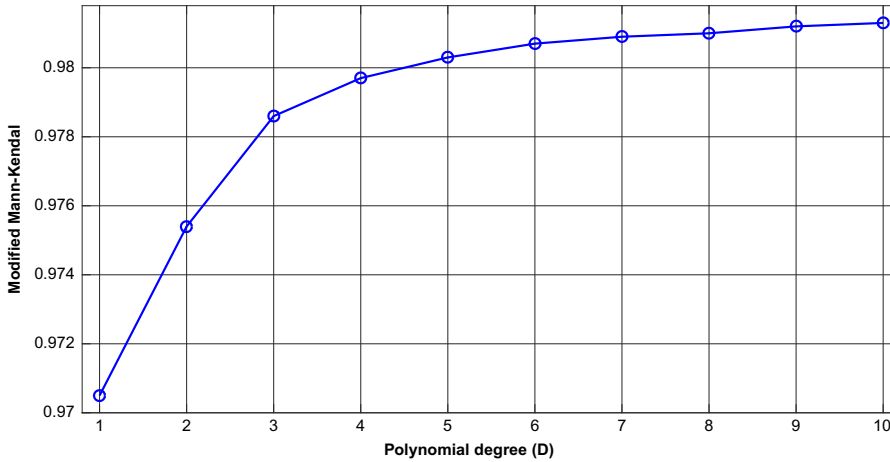

Fig. 20.11 Modified Mann-Kendal value vs the polynomial degree.

Table 20.2 Optimization results for $M = 5$

	AE^0	AE^1	AE^2	AE^3	AE^4	AE^5
DIC^0	−39,955	−953,757	−743,892	471,0798	882,5275	1,985,843
DIC^1	−783,606	1,989,894	−746,044	381,3022	−344,348	0
DIC^2	412,001	411,5522	271,9862	829,036	0	0
DIC^3	−922,063	−183,044	−16,7071	0	0	0
DIC^4	292,6789	906,5035	0	0	0	0
DIC^5	336,2406	0	0	0	0	0

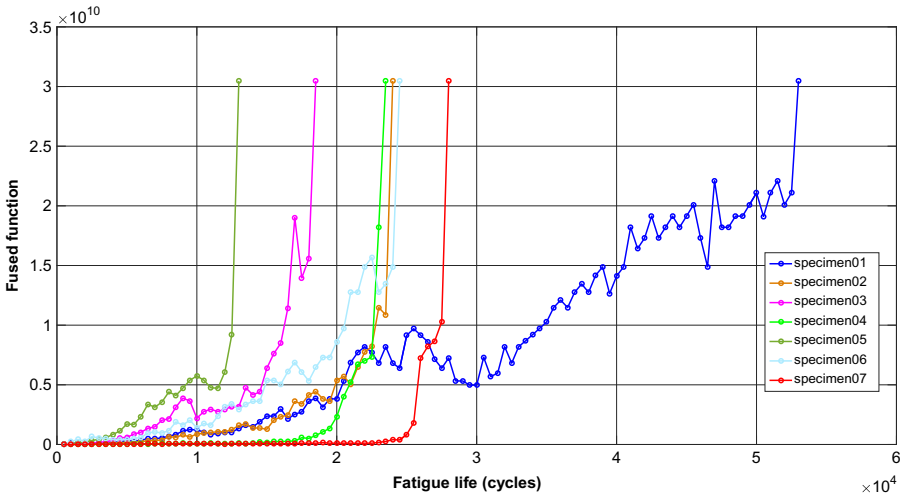

Fig. 20.12 Fused degradation histories of seven open-hole specimens.

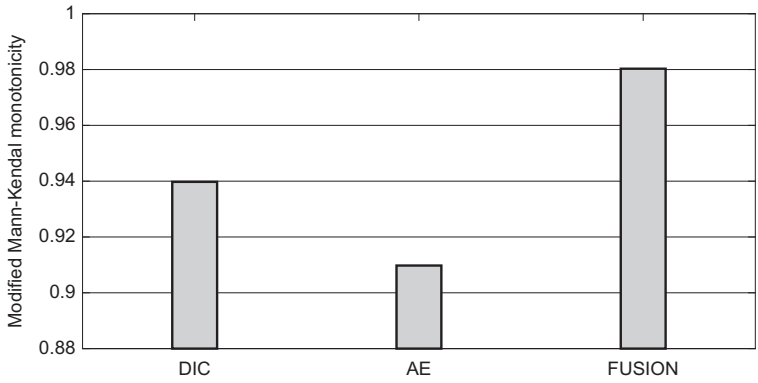

Fig. 20.13 Comparison between DIC, AE, and fusion MMK monotonicity.

histories in order to estimate the NHHSMM's parameters $\boldsymbol{\theta}$ and keeps the seventh degradation history as the testing prognostic dataset.

The mean/median RUL and the 90% confidence intervals can be calculated using Eq. (20.5). The level of confidence intervals depends on the application, that is, for aerospace applications 90% and 95% are common values [37] and 90% will be adopted for this study. Figs. 20.15–20.18 present the RUL estimations of the three available SHM techniques for specimen02, specimen03, specimen04, and specimen06, respectively.

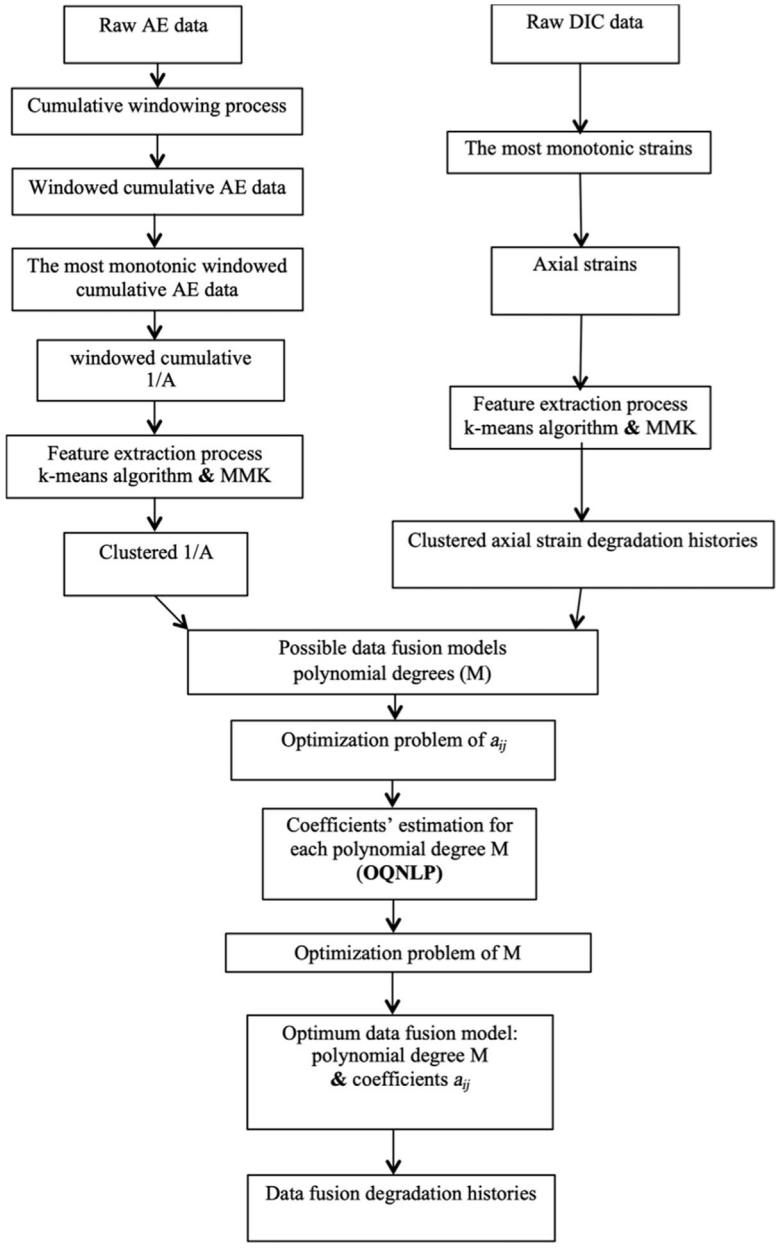

Fig. 20.14 The data fusion process.

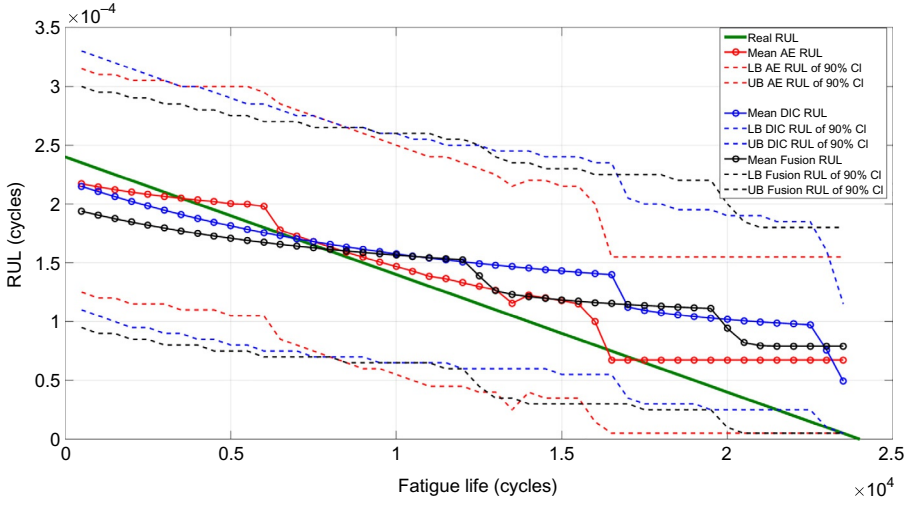

Fig. 20.15 Estimated mean RUL and 90% confidence intervals for specimen02.

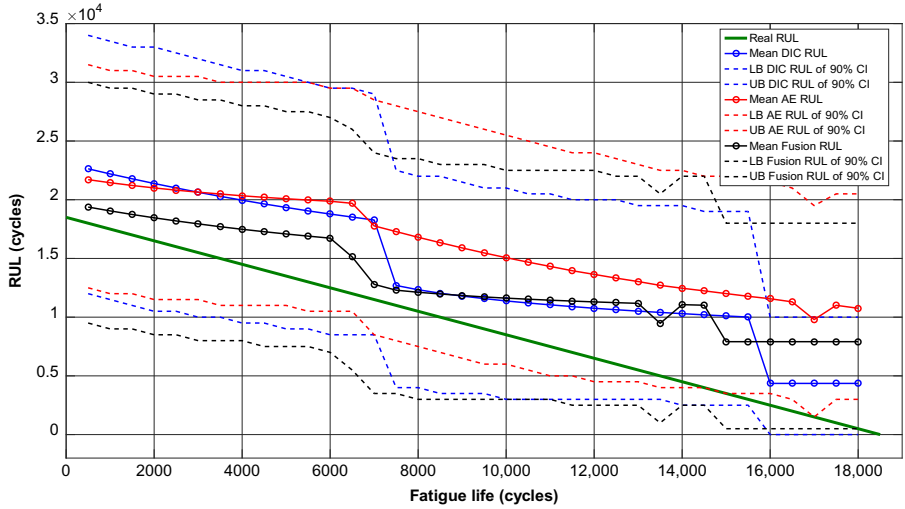

Fig. 20.16 Estimated mean RUL and 90% confidence intervals for specimen03.

The RUL estimations converge quite satisfactorily with the real (experimental) RUL values. Based on the results shown in Figs. 20.15–20.18 the strain data provide the best RUL estimations, while fused data and AE provide fair results.

20.5.5 Performance metrics

In order to quantify which data provide better predictions and validate or not the observations made for Figs. 20.15–20.18, various prognostic performance metrics are

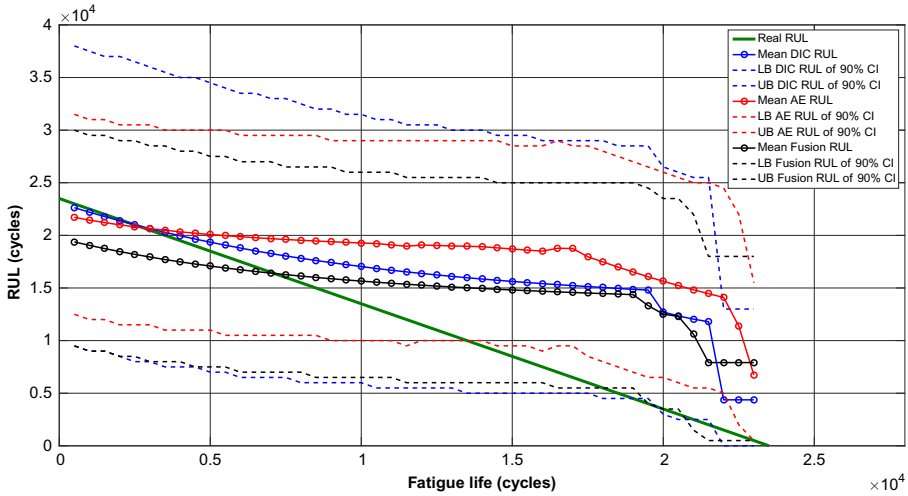

Fig. 20.17 Estimated mean RUL with 90% confidence intervals for specimen04.

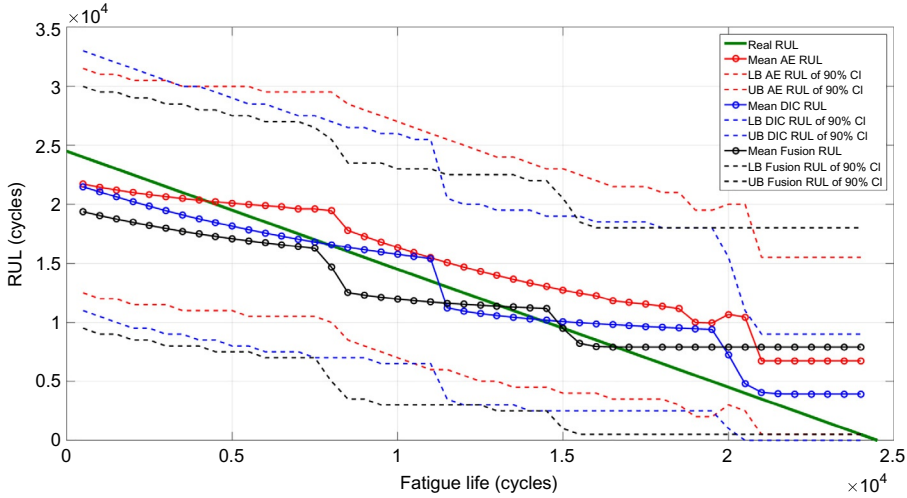

Fig. 20.18 Estimated mean RUL with 90% confidence intervals for specimen06.

employed for the comparison. Eight prognostic performance metrics are used to evaluate the predictive performance of the three NHHSMMs trained with the different types of SHM features. Six of them are metrics widely used in the literature; precision, mean squared error (MSE), mean absolute percentage error (MAPE), median absolute percentage error (MdAPE), cumulative relative accuracy (CRA), and convergence (C_{Em}) [51, 52]. The last two metrics monotonicity and confidence intervals distance convergence (CIDC) were very recently introduced by Eleftheroglou et al. [53].

A brief description of these two new metrics is provided hereafter. The aforementioned prognostic performance metrics are defined in the following:

1. Precision

   $\text{Precision} = \sqrt{\frac{\sum_{i=1}^{D}\left(E_m(t_i) - \overline{E_m}(t_i)\right)^2}{D-1}}$, where $\overline{E_m}$ is the mean value of error E_m and $E_m(t_i) = RUL_{actual}(t_i) - meanRUL(t_i)$ and $t_i \in [1,D]$ is the discrete time moment when the ith SHM observation is recorded.
2. Mean Squared Error (MSE)

   $\text{MSE} = \sqrt{\frac{\sum_{i=1}^{D}(E_m(t_i))^2}{D}}$.
3. Mean Absolute Percentage Error (MAPE)

   $\text{MAPE} = \frac{1}{D}\sum_{i=1}^{D}\left|\frac{100 \cdot E_m(t_i)}{RUL_{actual}(t_i)}\right|$.
4. Median Absolute Percentage Error (MdAPE)

   $\text{MdAPE} = \frac{1}{D}\sum_{i=1}^{D}\left|\frac{100 \cdot E_{md}(t_i)}{RUL_{actual}(t_i)}\right|$, where $E_{md}(t_i) = RUL_{actual}(t_i) - \text{medianRUL}(t_i)$.
5. Cumulative Relative Accuracy (CRA)

   $\text{CRA} = \frac{\sum_{i=1}^{D} RA(t_i)}{D}$ where $RA(t_i) = 1 - \left|\frac{E_m(t_i)}{RUL_{actual}(t_i)}\right|$.
6. Convergence (C_{Em})

   $C_{Em} = \sqrt{(x_c - t_1)^2 + y_c{}^2}$.

where

$$x_c = \frac{\sum_{\mathrm{i}=1}^{\mathrm{D}-1}\left(t_{i+1}{}^2 - t_i{}^2\right) \cdot |E_m(\mathrm{i})|}{2 \cdot \sum_{\mathrm{i}=1}^{\mathrm{D}-1}(t_{i+1} - t_i) \cdot |E_m(\mathrm{i})|} \text{ and } y_c = \frac{\sum_{\mathrm{i}=1}^{\mathrm{D}-1}(t_{i+1} - t_i) \cdot E_m(\mathrm{i})^2}{2 \cdot \sum_{\mathrm{i}=1}^{\mathrm{D}-1}(t_{i+1} - t_i) \cdot |E_m(\mathrm{i})|}.$$

7. Monotonicity

   The prognostic's function monotonicity can be measured based on the proposed MMK monotonicity criterion where $y(t_i)$ is replaced with $meanRUL(t_i)$. In case of the studied function, which is the RUL prediction function, the preferable value of MMK = −1 since it is expecting that the composite structure's RUL is decreasing monotonically during its lifetime.
8. Confidence Intervals Distance Convergence (CIDC)

   Goebel et al. [54] stated that as the amount of data increases during the fatigue life, the confidence intervals distance should converge. In order to quantify this statement, a new metric is introduced; the CIDC. This metric is an extension of the metric of convergence in Ref. [51] but in this case the centroid is under the confidence intervals distance curve. In general, lower Euclidian distance means faster convergence. Let (x_c, y_c) be the center of mass of the area under the confidence intervals distance curve, then the CIDC can be represented by the Euclidean distance between the (x_c, y_c) and the origin $(t_1,0)$, where

   $\text{CIDC} = \sqrt{(x_c - t_1)^2 + y_c{}^2}$

where

$$x_c = \frac{\sum_{i=1}^{D-1} (t_{i+1}{}^2 - t_i{}^2) \cdot (UCI(i) - LCI(i))}{2 \cdot \sum_{i=1}^{D-1} (t_{i+1} - t_i) \cdot (UCI(i) - LCI(i))}, y_c$$
$$= \frac{\sum_{i=1}^{D-1} (t_{i+1} - t_i) \cdot (UCI(i) - LCI(i))^2}{2 \cdot \sum_{i=1}^{D-1} (t_{i+1} - t_i) \cdot (UCI(i) - LCI(i))}$$

and *UCI*, *LCI*, the upper and lower selected confidence intervals, respectively.

The optimum values of the prognostic performance metrics are as follows and are presented in Tables 20.3–20.6 for all the specimens:

Precision: minimum value	CRA: maximum value
MSE: minimum value	Monotonicity: minimum value
MAPE: minimum value	C_{Em}: minimum value
MdAPE: minimum value	CIDC: minimum value

The best scores are highlighted and underlined.

Based on the results, the model that uses strain data as health monitoring features outperforms for most of the performance metrics. Data fusion also scores better for at least one RUL estimation for all the metrics except the last one. Especially the results of the monotonicity demonstrate the potential of the data fusion to provide features with very strong monotonic behavior, which is a key factor for the success of the prognostics output.

Table 20.3 Prognostic performance metrics (Precision and MSE)

	Precision			**MSE**		
	AE	**DIC**	**Fusion**	**AE**	**DIC**	**Fusion**
SP1	10,242.2	10,321.1	12,158.0	313,929,177	398,746,894	400,438,288
SP2	1839.0	3178.1	3406.1	5,157,196	17,305,198	14,521,109
SP3	1599.5	1517.0	1803.2	49,833,377	13,801,781	17,525,406
SP4	4696.9	1517.0	4359.4	65,596,414	13,801,781	29,438,165
SP5	1359.8	2264.5	1118.1	123,908,090	55,856,930	46,194,571
SP6	2265.6	1916.9	3263.6	11,177,939	3,747,730	10,439,022
SP7	4201.6	5444.5	5976.0	26,771,274	30,611,449	36,091,801

Precision: strain and AE data score better for 3 RUL estimations each and fusion data scores better for 1 RUL.
MSE: strain and AE data score better for 3 RUL estimations each and fusion data scores better for 1 RUL.

Table 20.4 Prognostic performance metrics (MAPE and MDAPE)

	MAPE			MDAPE		
	AE	**DIC**	**Fusion**	**AE**	**DIC**	**Fusion**
sp1	19.34	46.40	15.09	40.47	60.69	38.59
sp2	68.14	94.09	92.79	29.46	64.03	50.66
sp3	19,737	75.61	128.70	159.12	41.35	75.82
sp4	172,01	75.61	119.41	141.58	41.35	79.56
sp5	312,69	231.87	203.34	261.58	183.01	134.87
sp6	82,82	35.36	71.01	46.50	8.37	28.19
sp7	33,05	111.26	94.46	2.45	87.19	59.67

MAPE: strain data scores better for 2 RUL estimations, AE and fusion data score better for 2 RUL estimations.
MDAPE: strain data scores better for 2 RUL estimations, AE and fusion data score better for 2 RUL estimations.

Table 20.5 Prognostic performance metrics (CRA and Monotonicity)

	CRA			Monotonicity		
	AE	**DIC**	**Fusion**	**AE**	**DIC**	**Fusion**
sp1	0.238	0.281	0.135	−1	−0.987	−0.999
sp2	0.300	0.026	−0.001	−0.999	−1	−1
sp3	−0.973	0.244	−0.287	−0.999	−1	−0.999
sp4	−0.727	0.243	−0.254	−0.997	−1	−1
sp5	−2.127	−1.319	−1.033	−1	−1	−1
sp6	0.153	0.578	0.138	−0.999	−1	−1
sp7	0.245	−0.269	−0.130	−0.998	−1	−1

CRA: strain data scores better for 4 RUL estimations, AE data scores better for 2 RUL estimations and fusion data scores better for 1 RUL estimation.
Monotonicity: strain data and fusion data performed equally for 5 RUL estimations and AE data scores better for 2 RUL estimations.

Table 20.6 Prognostic performance metrics (C_{Em} and CIDC)

	C_{Em}			CIDC		
	AE	**DIC**	**Fusion**	**AE**	**DIC**	**Fusion**
sp1	15,872	17,405	15,054	24,486	21,450	25,136
sp2	18,518	19,171	24,456	10,898	10,823	11,278
sp3	9766	8456	10,657	8661	7712	8529
sp4	15,746	8456	19,675	11,334	7712	11,094
sp5	6208	5599	5670	6041	5555	5820
sp6	17,548	43,742	63,208	11,343	10,274	11,349
sp7	4491	51,975	63,950	12,678	12,853	13,282

C_{Em}: strain and AE data score better for 3 RUL estimations each and fusion data scores better for 1 RUL estimation.
CIDC: strain data scores better for 6 RUL estimations and AE data scores better for 1 RUL estimation.

20.6 Conclusions

The structural prognostics research field is a new dynamically rising field and it becomes more known, especially to the research and engineering community that works on the operation and maintenance, as it is a core element for the successful implementation of a condition-based maintenance framework. A great example is the very recently, funded under the European Union's Horizon 2020 research and innovation program, real-time condition-based maintenance for adaptive aircraft maintenance planning (ReMAP—https://h2020-remap.eu/) project, grant agreement No 769288, where one of the main objectives is the development of health prognostics of aircraft composite structures using innovative data-driven machine learning algorithms.

The main objective of the structural prognostics is to provide real-time estimations of the RUL of structures by blending machine learning algorithms, health monitoring data, and mechanics in order to design a prognostics framework. For the prediction of the RUL of composite structures subjected to fatigue loading, two types of prognostics frameworks have been developed. The first one uses physics-based algorithms while the second one uses data-driven algorithms.

In this chapter, a data-driven probabilistic framework for the in-situ prognostics of composite structures subjected to fatigue loading was presented. The framework is able to provide real-time estimation of the RUL of composite structures by combining health monitoring data and the multistate degradation NHHSMM. Two different sources of health monitoring data, AE, and strain data, on a feature-level, were presented. Open-hole carbon/epoxy specimens were subjected to constant amplitude fatigue loading up to failure and DIC and AE techniques were employed, to monitor the fatigue tests and provide the required data. In addition, eight prognostic performance metrics were employed in order to compare the performance of the RUL estimations.

A new data fusion approach was developed and the main objective was to produce hyper-features with high monotonicity. Although the degradation histories of the fused data had monotonicity higher than the monotonicity of the degradation histories of DIC and AE features, the fuse data did not provide always better estimations, indicating that the requirement of monotonicity is not enough and extra criteria should be involved. Nevertheless, the results demonstrate the potential of the proposed data fusion methodology and its evolvement by adding extra criteria, such as trendability, will enhance the performance of the fused data.

In order to accommodate the phenomenon of the structural degradation over time and the belief that as the amount of data increases the confidence intervals should converge, two prognostic performance metrics, MMK monotonicity, and CIDC were very recently proposed by the authors and materialized these statements. Their results were similar to the results of the other metrics and their applicability was verified.

The feature extraction process for the strain data was straightforward, as after the determination of the critical specimen's point, the axial strain data were extracted via the DIC technique. The well-established analytical model of Lekhnitskii enhanced the feature performance indicating that mechanics can play an informative role on the

feature selection process. These results can be used in future toward the development of a hybrid model where mechanics can play a key role for the feature extraction process.

Considering the importance of delivering a RUL prediction methodology that is generic enough and able to provide reliable real-time estimations, future research should focus mainly on two topics:

- Data fusion processes
- Real time uncertainty quantification

As discussed in Section 20.4.2, data fusion can be performed in three levels. There is not yet an established data fusion method that provides features, which enhance the RUL predictions significantly. Toward that direction, research should be performed on the selection and combination of appropriate SHM technologies, which will produce data that compliments each other and will enable the design of a super-feature that should fulfill the criteria of monotonicity, trendability, and prognosability. The prognostics framework should be flexible enough in order to accommodate any real time uncertainty, that is, unexpected loading event such as impact, which may dramatically change the operation life of the structure. This is important especially for the data-driven algorithms where the training of the algorithm is usually based on forecasted loading conditions. The algorithm should be designed in such a way that can recognize the change in the data histories and incorporate its effect on the analysis of the RUL.

References

[1] K.L. Reifsneider, A. Talug, Analysis of fatigue damage in composite laminates, Int. J. Fatigue 2 (1980) 3–11.
[2] T. Philippidis, A.P. Vassilopoulos, Life prediction methodology for GFRP laminates under spectrum loading, Compos. Part A 35 (2004) 657–666.
[3] M. Quaresimin, L. Susmel, R. Talreja, Fatigue behaviour and life assessment of composite laminates under multiaxial loadings, Int. J. Fatigue 32 (2010) 2–16.
[4] R. Sarfaraz, A.P. Vassilopoulos, T. Keller, A hybrid S-N formulation for fatigue life modeling of composite materials and structures, Compos. Part A 43 (2012) 445–453.
[5] W. van Paepegem, J. Degrieck, A new coupled approach of residual stiffness and strength for fatigue of fibre-reinforced composites, Int. J. Fatigue 24 (2002) 747–762.
[6] V. van Paepegem, J. Degrieck, Coupled residual stiffness and strength model for fatigue of fibre-reinforced composite materials, Compos. Sci. Technol. 62 (2002) 687–696.
[7] C. Kassapoglou, Fatigue of composite materials under spectrum loading, Compos. Part A 41 (2010) 663–669.
[8] M. Shokrieh, L. Lessard, Progressive fatigue damage modeling of composite materials, Part I: modeling, J. Compos. Mater. 34 (2000) 1056–1080.
[9] M.M. Shokrieh, F.T. Behrooz, A unified fatigue life model based on energy method, Compos. Struct. 75 (2006) 444–450.
[10] S. Haojie, Y. Weixing, W. Yitao, Synergistic damage mechanic model for stiffness properties of early fatigue damage in composite laminates, Procedia Eng. 74 (2014) 199–209.

[11] B. Mohammadi, H. Pakdel, Fatigue driven matrix crack propagation in laminated composites, Mater. Des. 146 (2018) 108–115.
[12] B. Mohammadi, H. Pakdel, Experimental and variational-based analytical investigation of multiple cracked angle-ply laminates, Eng. Fract. Mech. 190 (2018) 198–212.
[13] A. Varvani-Farahani, H. Haftchenari, M. Panbechi, An energy-based fatigue damage parameter for off-axis unidirectional FRP composites, Compos. Struct. 79 (3) (2007) 381–389.
[14] J. Varna, R. Joffe, N.V. Akshantala, R. Talreja, Damage in composite laminates with off-axis plies, Compos. Sci. Technol. 59 (1999) 2139–2147.
[15] N.-H. Kim, D. An, J.-H. Choi, Prognostics and Health Management of Engineering Systems: An Introduction. Springer, 2017. https://doi.org/10.1007/978-3-319-44742-1.
[16] H.M. Elattar, H.K. Elminir, A.M. Riad, Prognostics: a literature review, Complex Intell. Syst. 2 (2016) 125–154.
[17] X.S. Si, W. Wang, C.H. Hu, D.H. Zhou, Remaining useful life estimation—a review on the statistical data driven approaches, Eur. J. Oper. Res. 213 (2011) 1–14.
[18] J. Chiachío, M. Chiachío, A. Saxena, S. Sankararaman, G. Rus, K. Goebel, Bayesian model selection and parameter estimation for fatigue damage progression models in composites, Int. J. Fatigue 70 (2014) 361–373.
[19] J. Chiachío, M. Chiachío, S. Sankararaman, A. Saxena, K. Goebel, Condition-based prediction of time-dependent reliability in composites, Reliab. Eng. Syst. Saf. 142 (2014) 134–147.
[20] M. Corbetta, C. Sbarufatti, M. Giglio, A. Saxena, K. Goebel, A Bayesian framework for fatigue life prediction of composite laminates under co-existing matrix cracks and delamination, Compos. Struct. 187 (2018) 58–70.
[21] J.A. Pascoe, R.C. Alderliesten, R. Benedictus, Methods for the prediction of fatigue delamination growth in composites and adhesive bonds—a critical review, Eng. Fract. Mech. 112 (2013) 72–96.
[22] A. Carpinteri, M. Paggi, A unified interpretation of the power laws in fatigue and the analytical correlations between cyclic properties of engineering materials, Int. J. Fatigue 31 (2009) 1524–1531.
[23] Y. Liu, S. Mohanty, A. Chattopadhyay, A Gaussian process based prognostics framework for composite structures, in: Proceedings of SPIE: Modeling, Signal Processing, and Control for Smart Structures, San Diego, 2009.
[24] Y. Liu, S. Mohanty, A. Chattopadhyay, Condition based structural health monitoring and prognosis of composite structures under uniaxial and biaxial loading, J. Nondestruct. Eval. 29 (2010) 181–188.
[25] N. Eleftheroglou, T.H. Loutas, Fatigue damage diagnostics and prognostics of composites utilizing structural health monitoring data and stochastic processes, Struct. Health Monit. 15 (2016) 473–488.
[26] N. Eleftheroglou, D. Zarouchas, T.H. Loutas, R. Alderliesten, R. Benedictus, Online remaining fatigue life prognosis for composite materials based on strain data and stochastic modeling, Key Eng. Mater. 713 (2016) 34–37.
[27] T.H. Loutas, N. Eleftheroglou, D. Zarouchas, A data-driven probabilistic framework towards the in-situ prognostics of fatigue life of composites based on acoustic emission data, Comp. Struct. 161 (2017) 522–529.
[28] C.R. Farrar, N.A.J. Lieven, Damage prognosis: the future of structural health monitoring, Phil. Trans. R. Soc. A 365 (2007) 623–632.
[29] C.R. Farrar, K. Worden, Structural Health Monitoring, a Machine Learning Prospective, John Wiley & Sons, Ltd, 2013.

[30] M. Saeedifar, M.A. Najafabadi, D. Zarouchas, H.H. Toudeshky, M. Jalalvand, Clustering of interlaminar and intralaminar damages in laminated composites under indentation loading using acoustic emission, Compos. Part B 144 (2018) 206–219.
[31] M. Saeedifar, M.A. Najafabadi, D. Zarouchas, H.H. Toudeshky, M. Jalalvand, Barely visible impact damage assessment in laminated composite using acoustic emission, Compos. Part B 152 (2018) 180–192.
[32] T.H. Loutas, A. Vavouliotis, P. Karapappas, V. Kostopoulos, Fatigue damage monitoring in carbon fiber reinforced polymers using the acousto-ultrasonics technique, Polym. Compos. 31 (2010) 1409–1417.
[33] D.M. Peairs, G. Park, D.J. Inman, Improving accessibility of the impedance-based structural health monitoring method, J. Intell. Mater. Syst. Struct. 15 (2004) 129–139.
[34] S. Bhalla, C. Soh, Electro-mechanical impedance technique, in: C.K. Soh, Y. Yang, S. Bhalla (Eds.), Smart Materials in Structural Health Monitoring, Control and Biomechanics, Springer, Berlin, Heidelberg, 2012, pp. 17–51.
[35] S. Takeda, Y. Aoki, T. Ishikawa, N. Takeda, H. Kikukawa, Structural Health Monitoring of Composite Wing During Durability Test, Compos. Struct. 79 (2007) 133–139.
[36] D.L. Hall, J. Llinas, An introduction to multisensor data fusion, Proc. IEEE 85 (1997) 6–23.
[37] X. Zhao, M. Li, G. Song, J. Xu, Hierarchical ensemble-based data fusion for structural health monitoring, Smart Mater. Struct. 19 (2010) 1 4–45.
[38] R. Moghaddass, M.J. Zuo, An integrated framework for online diagnostic and prognostic health monitoring using a multistate deterioration process, Reliab. Eng. Syst. Saf. 124 (2014) 92–104.
[39] R. Moghaddass, M.J. Zuo, Multistate degradation and supervised estimation methods for a condition-monitored device, IIE Trans. 46 (2014) 131–148.
[40] J. Coble, H.J. Wesley, Identifying optimal prognostic parameters from data: a genetic algorithms approach, in: Annual Conference of the Prognostics and Health Management Society, 2009.
[41] F. Qian, G. Niu, Remaining useful life prediction using ranking mutual information based monotonic health indicator, in: Prognostics and System Health Management Conference, September, 2015.
[42] L. Liao, Discovering prognostic features using genetic programming in remaining useful life prediction, IEEE Trans. Ind. Electron. 61 (2014) 2464–2472.
[43] D. McCarter, B. Shumaker, B. McConkey, H. Hashemian, Nuclear power plant instrumentation and control cable prognostics using indenter modulus measurements, Int. J. Prognos. Health Manag. 16 (2014) 1–10.
[44] L. Yaguo, Intelligent Fault Diagnosis and Remaining Useful Life Prediction of Rotating Machinery, Butterworth-Heinemann, 2016.
[45] H. Jegou, M. Douze, C. Schmid, Product quantization for nearest neighbor search, IEEE Trans. Pattern Anal. Mach. Intell. 33 (2011) 117–128.
[46] S.-F. Jiang, C.-M. Zhang, S. Zhang, Two-stage structural damage detection using fuzzy neural networks and data fusion techniques, Expert Syst. Appl. 38 (2011) 511–519.
[47] X.E. Gros, Multisensor data fusion and integration in NDT, in: Applications of NDT Data Fusion, Springer, US, 2001, pp. 1–12.
[48] D.L. Hall, S.A.H. McMullen, Mathematical Techniques in Multi-Sensor Data Fusion, Artech House, Boston, 2004.
[49] D.L. Hall, J. Llinas, An introduction to multisensor data fusion, Proc. IEEE 85 (1997) 6–23.

[50] S.G. Lekhnitskii, S.W. Tsai, T. Cheron, Anisotropic Plates, Gordon and Breach Science Publishers, New York, 1963.
[51] A. Saxena, J. Celaya, B. Saha, S. Saha, K. Goebel, Metrics for offline evaluation of prognostic performance, Int. J. Prognos. Health Manag. 1 (2010) 1–20.
[52] T. Peng, J. He, Y. Xiang, Y. Liu, A. Saxena, J. Celaya, K. Goedel, Probabilistic fatigue damage prognosis of lap joint using Bayesian updating, J. Intell. Mater. Syst. Struct. 26 (2014) 965–979.
[53] N. Eleftheroglou, D. Zarouchas, T.H. Loutas, R.C. Alderliesten, R. Benedictus, Structural health monitoring data fusion for in-situ prognosis of composite structures, Reliab. Eng. Syst. Saf. 178 (2018) 40–54.
[54] K. Goebel, B. Saha, A. Saxena, A comparison of three data-driven techniques for prognostics, in: 62nd Meeting of the Society for Machinery Failure Prevention Technology, 2008.